V European Conference on Computational Fluid Dynamics
ECCOMAS CFD 2010
J. C. F. Pereira and A. Sequeira (Eds)
Lisbon, Portugal,14-17 June 2010

ANALYSIS OF UNSTEADINESS IN TRANSONIC SHOCK/BOUNDARY LAYER INTERACTIONS

M. Bernardini*, S. Pirozzoli* and F. Grasso*

*Università di Roma "La Sapienza",
Via Eudossiana, 18, 00184 Roma
e-mail: {sergio.pirozzoli, matteo.bernardini,francesco.grasso}@uniroma1.it

Key words: Shock waves, Transonic flows, Turbulent boundary layers

Abstract. *The unsteady effects in the interaction of a turbulent boundary layer with a normal shock wave are investigated exploiting a direct numerical simulation (DNS) database at free-stream Mach number $M_\infty = 1.3$ and Reynolds number $Re_\theta \approx 1200$ (based on the momentum thickness of the upstream boundary layer), corresponding to conditions of incipient mean flow separation. As found in experiments, the mean flow pattern consists of an upstream fan of compression waves associated with the thickening of the boundary layer, and the supersonic region is terminated by a nearly-normal shock, with substantial bending of the interacting shock. At the selected conditions the flow does not exhibit separation in the mean. However, the interaction region is characterized by (strongly unsteady) instantaneous flow reversal in a zone extending for many (upstream) boundary layer thicknesses past the nominal location of the interacting shock, and by the formation of a turbulent mixing layer, with associated release of vortical structures. The flow in the relaxation zone past the shock exhibits a self-similar structure, characterized by constancy of a modified pressure gradient parameter.*

1 INTRODUCTION

The interactions of shock waves with turbulent boundary layers (SBLI) are frequently encountered in transonic and supersonic flows, and they have been the subject of extensive research over the last decades[9,5,7,12]. Although significant advances have been made, some physical processes are not yet fully understood, mainly related to the mechanisms responsible for the amplification of disturbances, and to the possible occurrence of low-frequency motion, that is observed for strong interactions[11,14].

Owing to difficulties encountered (both in experiments and in computations) in anchoring the shock wave, and to the strong sensitivity to the downstream flow conditions, transonic interactions have received comparatively less attention in comparison with canonical supersonic interactions, such as impinging shocks and compression ramps. A comprehensive review of SBLI in the transonic regime was reported by[5], who collected a large amount of experimental information related to normal shock/boundary layer interactions in several configurations (including transonic airfoils, nozzles, bumps in transonic wind tunnels). Those authors found that the boundary between weak and strong interactions is weakly dependent upon the Reynolds number of the flow (as long as the boundary layer is fully developed), and incipient mean flow separation occurs at $M_\infty \approx 1.3$.

Transonic SBLI in a channel with wall-mounted bump were experimentally investigated by[6], who considered shock strengths in the range $M_\infty = 1.3 - 1.45$, corresponding to conditions from incipient separation to extensively separated flow. The experiments showed the development of strong anisotropy in Reynolds stresses caused by a different amplification of the tangential and normal components, whose maxima were found to occur well away from the wall. The experiments also revealed the occurrence of a relaxation process, that drives back the flow towards a new equilibrium state on a slow time-scale related to the lifetime of the large vortical structures that are formed through the interaction. Bruce [1] carried out an experimental study of forced and unforced transonic SBLI in a rectangular channel, both with and without control. The steady data at $M_\infty = 1.3$, $Re_\theta \approx 10^4$ show a pattern typical of a weak SBLI, with a weak compression fan ahead of the main shock, and attached flow throughout the interaction region.

A limited number of large-eddy simulations (LES) has been performed for two-dimensional bump configurations in transonic channels. Sandham et al. [20] performed LES of a transonic turbulent boundary layer over a circular-arc bump (corresponding to an upstream Mach number $M_\infty \approx 1.16$) using the dynamic Smagorinsky model, and a synthetic turbulence technique to enforce transition to a fully turbulent state. Those authors concluded that the shock wave is very nearly steady, and the level of turbulence anisotropy in the flow past the interaction is not very high. Such discrepancy was ascribed by those authors to problems encountered by the Smagorinsky model to capture the rapid rise and fall of turbulence levels in the separated shear layer developing under the interacting shock.

The first direct numerical simulation of transonic SBLI has recently been reported by the present authors[17], who considered the interaction of a normal shock wave with

a supersonic turbulent boundary layer flow at $M_\infty = 1.3$, $Re_\theta \approx 1200$. The aim of the present work is to exploit the DNS database to shed some light on the physical phenomena involved in transonic interactions with emphasis on the unsteady features as well as on the onset of large scale vortical structures.

NUMERICAL METHODOLOGY

The computational strategy to solve the governing equations relies on a modification of a conservative finite-difference algorithm that has been extensively validated in previous works both for isotropic decaying compressible turbulence and for wall bounded turbulent supersonic flows[18,19,16]. In the smooth parts of the flow field the convective fluxes are discretized by means of a linear seventh-order central upstream approximation with local Lax-Friedrichs flux splitting, whereas near shock transitions a fifth-order WENO reconstruction is activated to rule out the onset of spurious Gibbs oscillations. As proposed in[15], the switch between linear and WENO reconstruction is carried out at the intermediate nodes of the computational mesh on the basis of the value of the density difference across the neighboring nodes ($\Delta\rho_{j+1/2} = \rho_{j+1} - \rho_j$). The WENO reconstruction is activated whenever the absolute value of $\Delta\rho$ becomes larger than a threshold value $\Delta\rho^*$, defined as

$$\frac{\Delta\rho^*}{\rho_\infty} = \varepsilon_1 + \frac{\varepsilon_2 - \varepsilon_1}{1 + M^{20}}, \tag{1}$$

where M is the local Mach number, and the constants are set to $\varepsilon_1 = 0.01$, $\varepsilon_2 = 0.5$. According to Eq. 1, a low threshold level ($\Delta\rho^* = \varepsilon_1$) is used in the supersonic part of the flow field, whereas a larger threshold ($\Delta\rho^* = \varepsilon_2$) is used in the subsonic part of the boundary layer, that does not support shock transitions. Such procedure effectively guarantees that the high-order linear reconstruction is used throughout the subsonic layer, while the more dissipative shock-capturing reconstruction is selectively applied to a very limited number of grid points.

The computational domain employed for the simulation has an overall size ($L_x \times L_y \times L_z$) = ($106\delta_{in} \times 427\delta_{in} \times 12.8\delta_{in}$) in the x (streamwise), y (wall-normal) and z (spanwise) directions, respectively, where δ_{in} is the boundary layer thickness at the inlet section (defined in terms of 99% of the outer velocity), and it is discretized with a grid consisting of $2561 \times 281 \times 351$ points. The grid points are uniformly spaced in the spanwise direction, whereas they are slightly clustered in the streamwise direction around the nominal location of the normal shock wave $x_s = 32\delta_{in}$. Grid points are clustered in the wall-normal direction according to a hyperbolic sine mapping up to $y/\delta_{in} = 8$, and according to a geometric progression up to the upper boundary of the computational domain. In terms of wall units the spanwise mesh spacing is $\Delta z^+ = 5.53$, whereas the streamwise and wall normal spacings are in the range $\Delta x^+ = 4.5 \div 7.75$ and $\Delta y^+ = 1.05 \div 42.5$. Note that wall units are defined in terms of the friction velocity and of the viscous length scale evaluated at the wall ($u_\tau = \sqrt{\tau_w/\rho_w}$, $\delta_v = \nu_w/u_\tau$) at the reference station $x_{ref}/\delta_{in} = 17.25$, chosen immediately upstream of the interaction zone, where the incoming boundary layer is

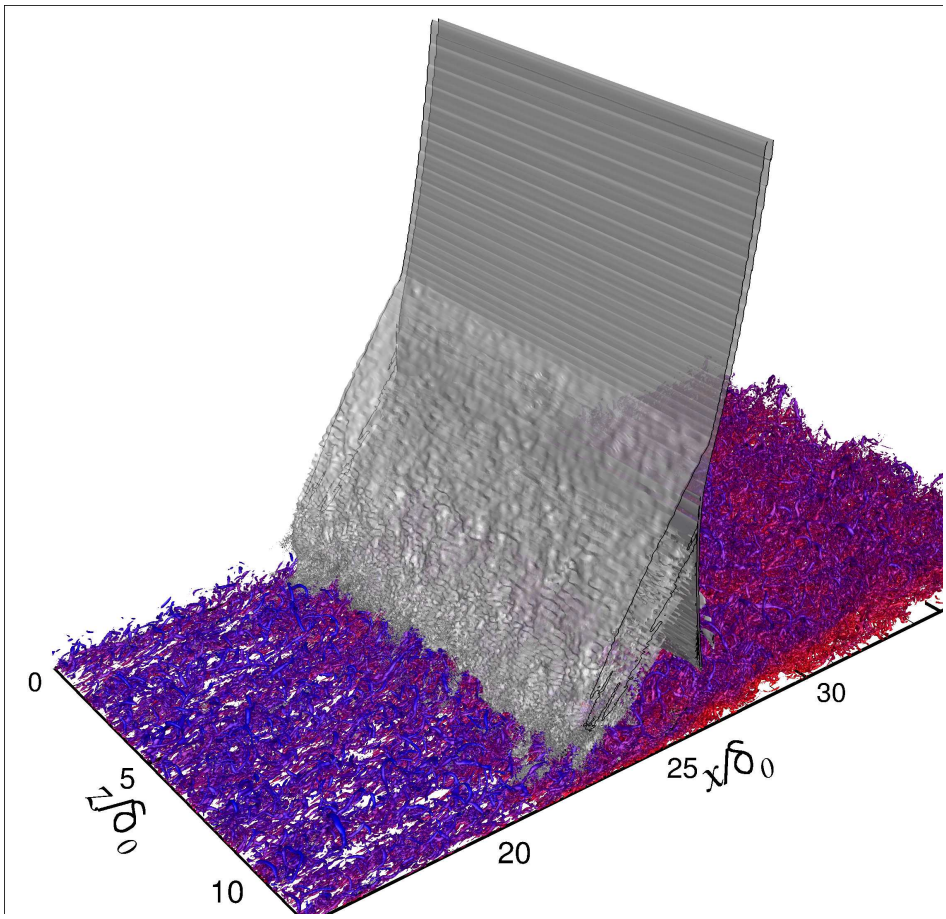

Figure 1: Three-dimensional view of transonic SBLI. Gray shades are used to indicate the shock system, and coloured contours to extract vortical structures. Axes are scaled with respect to the incoming boundary layer thickness (δ_0).

unperturbed and fully turbulent.

For clarity in the illustration of results, the data will be reported by setting the origin of the longitudinal coordinate at the location (x_0) where the mean wall pressure starts to rise, here conventionally determined as the point where $\overline{p}_w = 1.005 p_\infty$. A relevant interaction length scale (L) is then defined as the distance between the point where the mean wall pressure equals its critical value (x_1, where 'sonic' conditions are attained) and x_0, and a scaled longitudinal coordinate is introduced, $x^* = (x - x_0)/L$.

2 Instantaneous flow visualizations

In this section we provide instantaneous flow field visualizations to highlight the general features of the interaction and its structure. In particular, to shed some light on the physical phenomena associated with transonic SBLI we report 2D and 3D visualizations obtained from instantaneous realizations of the flow. In figure 1 a rendered view of the

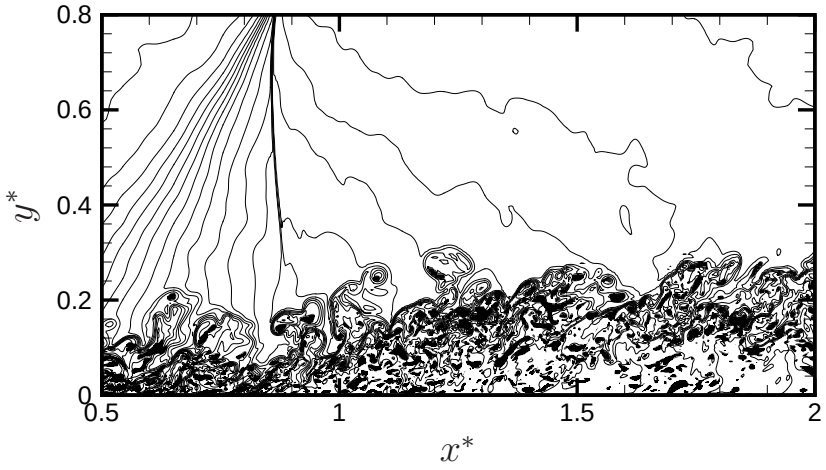

Figure 2: Instantaneous visualization of vortex shedding in the mixing layer region. Solid lines depict isocontour levels of density ($0.75 \leq \rho/\rho_\infty \leq 1.55$); grey patches correspond to vortex structures identified according to the swirling strength criterion.

shock system at a given time instant is depicted. For that purpose, the shock system (in gray shades) is identified as an iso-surface of the Ducros sensor, and vortical structures are educed as iso-surfaces of the swirling strength ($\lambda_{ci} = 1.6\, u_\infty/\delta_0$), and coloured with the local Mach number (levels from 0 to 1.3, colour scale from blue to violet). The figure well highlights the three-dimensional character of the lambda-like interaction pattern. The shock wave is significantly distorted by the presence of the boundary layer and it is affected by the incoming structures, that cause the spanwise wrinkling of the upstream compression fan in a way that resembles the visualizations of Wu and Martin [23] in compression corner interactions. The figure also shows the presence of elongated vortices dominating upstream of the interaction, and it reveals the onset of larger coherent structures in the interaction region, associated with the formation of a mixing layer. This scenario is also confirmed by figure 2, showing a zoom of vortex structures in the streamwise/wall-normal plane. This representation allows to appreciate the release of vortices taking place mainly in the supersonic region, upstream of the foot of the rear shock.

The computed instantaneous slices of the pressure, streamwise velocity and density fields are shown in figure 3. The maps highlight the presence of ordered (coherent) structures evolving inside the boundary layer upstream of the interaction. In particular, sharp density interfaces having a strong three-dimensional character are apparent in the density field in the outermost part of the boundary layer, corresponding to outer layer bulges. Additional large structures are also observed in the instantaneous pressure field, corresponding to local pressure dips. These structures are associated with the inflection points in the instantaneous velocity distribution via the Kelvin-Helmholtz instability mechanism, lifting away from the wall in proximity of the foot of the incoming shock, and propagating downstream to form a mixing layer embedded in the interaction zone. A similar shedding of coherent structures was also observed by Souverein et al. [22] in the case of an oblique

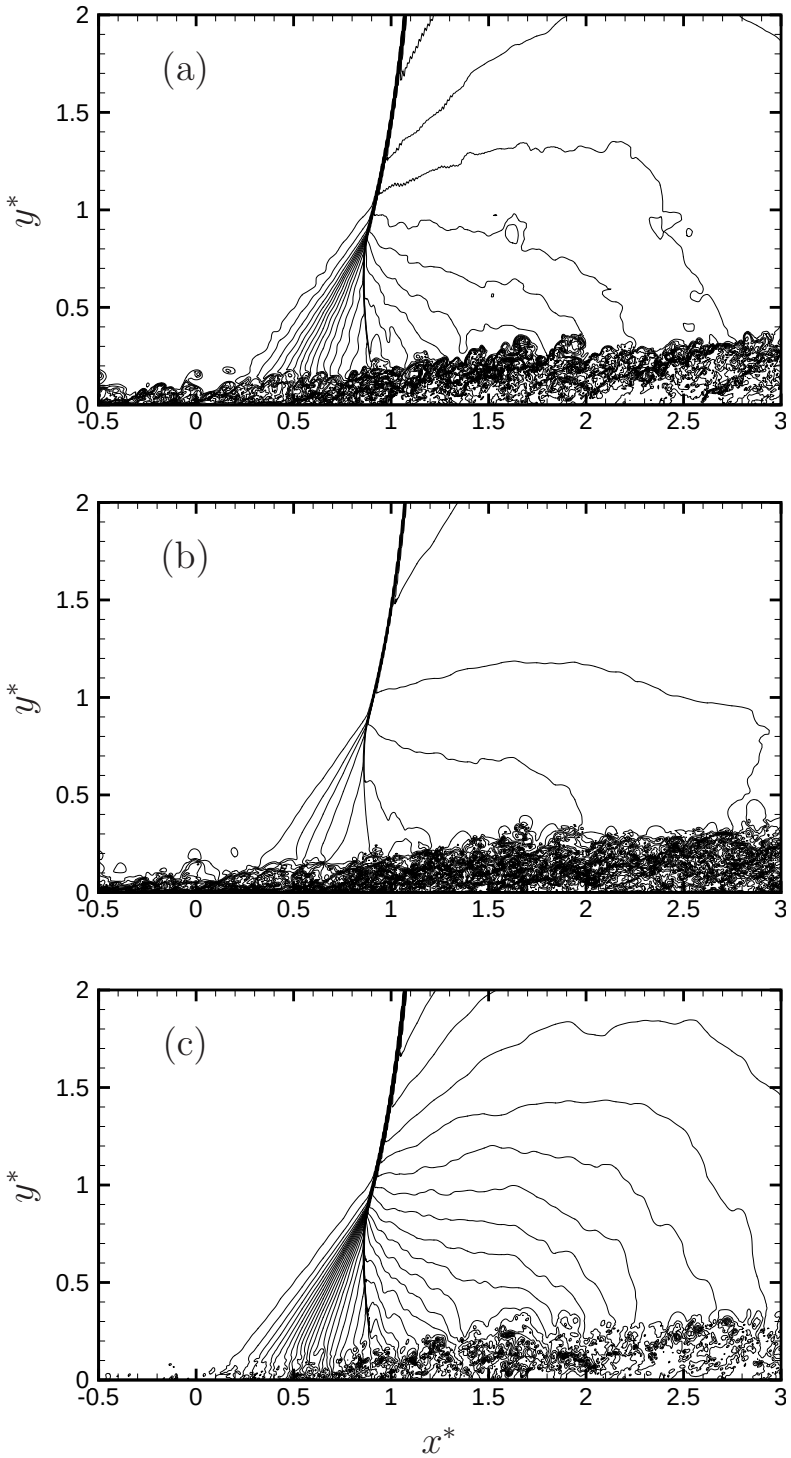

Figure 3: Instantaneous fields of (a) density, (b) streamwise velocity and (c) pressure in $x - y$ plane.

shock impinging on a solid wall and by Na and Moin [13] for a separated low-speed turbulent boundary layer.

3 Mean flow properties

The computed average fields of pressure, density and Mach number, reported in figure 4, show a pattern consistent with previous experimental observations[8] at the same upstream Mach number. The mean shock pattern consists of the interacting shock, which is observed to bend significantly while approaching the wall, and a fan of compression waves originated well upstream of the nominal impingement point, terminated by a nearly normal shock foot. The sonic point lies very close to the foot of the rear shock and the triple point is in the supersonic region at a distance of approximately one interaction length scale from the wall. The flow downstream of the shock foot is subsonic, and the presence of a supersonic tongue is not observed. The most evident effect of the interaction is the thickening of the boundary layer, and the (obvious) increase of mean density and pressure. the formation of a mixing layer is also visible from the mean pressure and density fields, that exhibit a dip past the interaction region at a distance of $0.1 \div 0.2L$ from the wall.

The distribution of the average skin friction coefficient $\overline{C}_f = \tau_w/q_\infty$ is shown in figure 5, where we also report (for the ZPG region) the skin friction correlations of Kármán-Schoenherr and Blasius[10], upon the van Driest II transformation. The figure shows that in the zero-pressure gradient region upstream of the interaction the skin friction slowly decreases, in agreement with the semi-empirical friction formulas (especially with the Blasius curve). Starting from $x^* = 0$, $\overline{C}_f$ exhibits a sudden drop, and attains a minimum (close to zero) at $x^* \approx 1.8\,L$, that approximately corresponds to the location of maximum H_i, where the boundary layer profile achieves the maximum distortion. The skin friction then exhibits a slow recovery past the interaction zone. Consistent with the claims of Delery and Marvin [5], the present case is to be classified as an incipient separation one.

4 UNSTEADY PROPERTIES

The analysis of the averaged skin friction coefficient in the previous section has shown that mean separation is absent in the present simulation. However, although no mean flow reversal is found, the adverse pressure gradient is sufficiently strong to locally cause scattered spots of reversed flow throughout the interaction. To get some insight into the dynamics of the flow reversal region, in figure 6 we report contours of the instantaneous skin friction coefficient C_f at a given time instant. The figure shows an overall view of the computational domain, and a zoom in the shock region. The iso-line $C_f = 0$ is also included as a solid line. The figure well highlights the strong intermittent character of the interaction region. The streaky structures of the ZPG region disappear owing to the adverse pressure gradient, and zones of negative instantaneous C_f are found starting from $x^* = 0.4$, all the way down to $x^* = 5$.

To give a complete and more quantitative picture of the reversed flow in figure 7 we

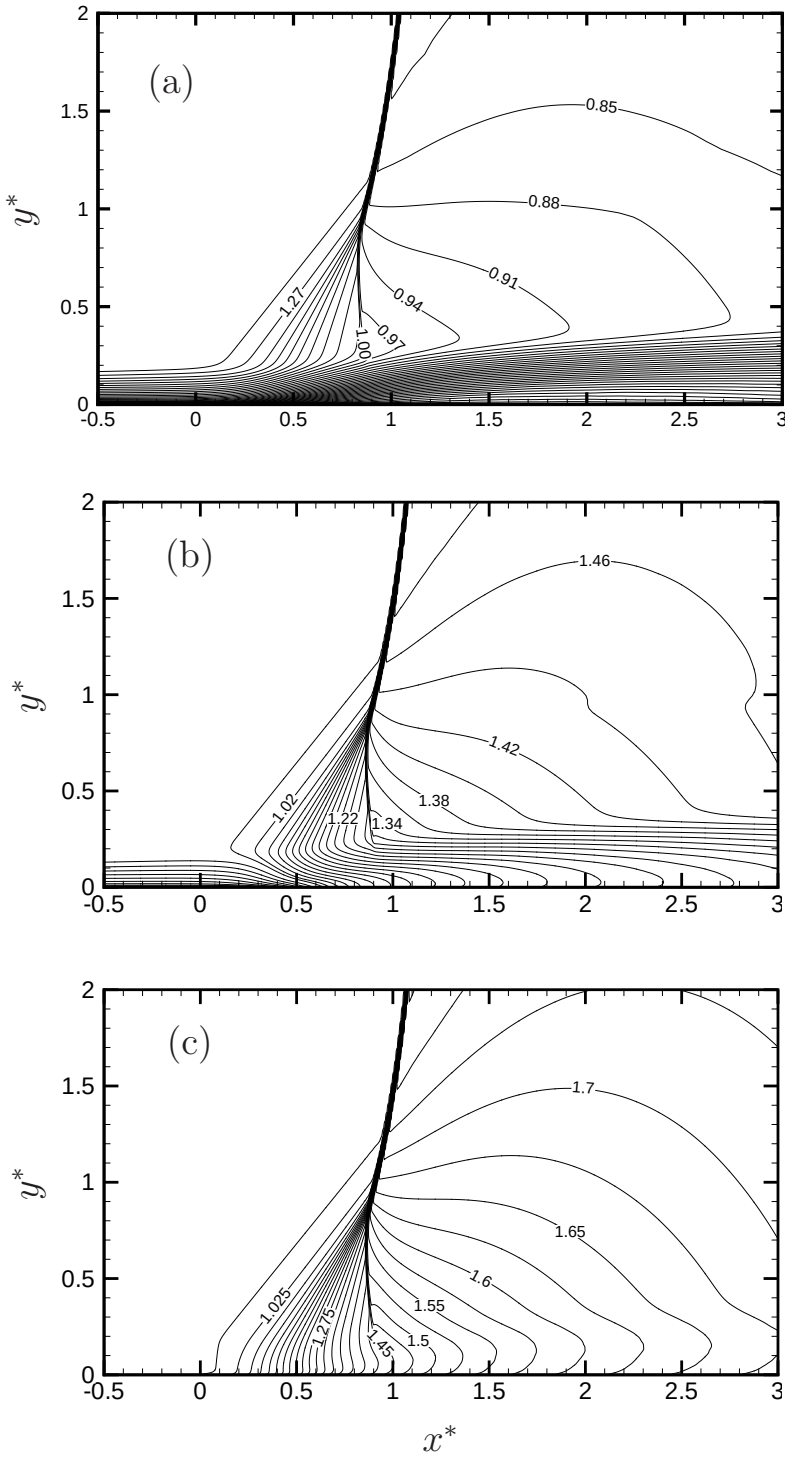

Figure 4: Average fields of (a) Mach number, (b) density $\overline{\rho}/\rho_\infty$ and (c) pressure $\overline{p}/p_\infty$.

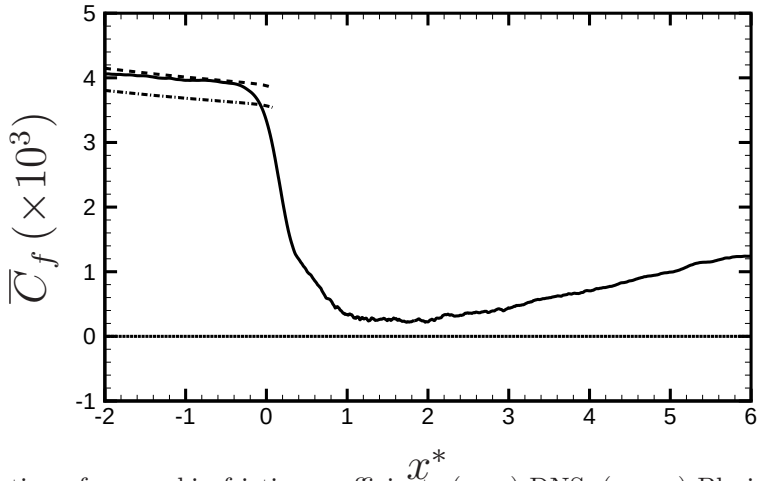

Figure 5: Distribution of mean skin friction coefficient. (——) DNS; (– – – –) Blasius; (- · - · -) Kármán-Schoenherr.

report the statistical frequency (indicated as $\overline{\gamma}$) of wall points with instantaneous back-flow (i.e. where the $\partial u/\partial y < 0$). Based on the fraction of time that the flow moves upstream,[21] provided a set of quantitative definitions of the detachment state near the wall for steady-freestream separating turbulent boundary layers: incipient detachment (ID) occurs with instantaneous back-flow 1% of the time ($\overline{\gamma} = 1\%$); intermittent transitory detachment (ITD) occurs with instantaneous back-flow 20 % of the time ($\overline{\gamma} = 20\%$); transitory detachment (TD) occurs with instantaneous back-flow 50 % of the time ($\overline{\gamma} = 50\%$). The same authors pointed out that, on the base of the available data, transitory detachment (TD) takes place at the same location as the detachment (D), defined on the basis of the zero shear stress criterion. Assuming such terminology, the distribution of $\overline{\gamma}$ in figure 7 shows that intermittent transitory detachment occurs at $x^* \approx 0.35$ and, consistently with the findings of the previous section, it confirms that detachment (or mean separation) does not occur.

5 ANALYSIS OF THE RECOVERY PROCESS

The state of the boundary layer past the interaction zone is here analyzed, with the objective to characterize the possible occurrence of 'universal' restoring mechanisms. Clauser [4] introduced a pressure gradient parameter

$$\beta = \frac{\delta^*}{\tau_w}\frac{\mathrm{d}\overline{p}}{\mathrm{d}x}, \tag{2}$$

and defined an equilibrium boundary layer as one where the parameter β is constant. In that case he was able to show that the velocity deficit normalized by the friction velocity is independent on the streamwise coordinate. The distribution of β obtained from the present DNS is shown in figure 8. Clauser's pressure gradient parameter is zero up to the origin of the interaction, then it increases sharply, with a peak $\beta = 8.7$ at $x^* \approx 0.5$, and

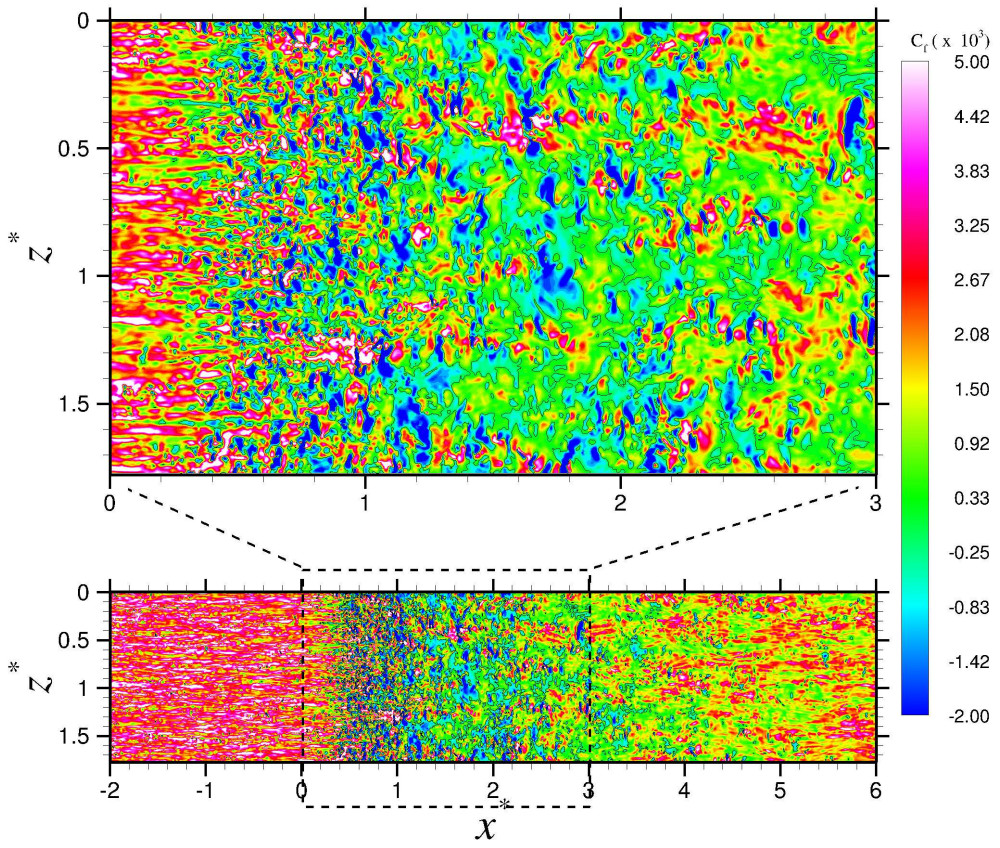

Figure 6: Contours of instantaneous skin friction (the solid line indicates the iso-line $C_f = 0$).

then it decreases monotonically up to the end of the computational domain. Therefore, according to Clauser's definition, the present APG flow is to be classified as strongly out of equilibrium throughout the interaction zone. Consistently, deficit profiles scaled by the friction velocity (shown in figure 10) do not collapse into a single curve.

Using a similarity analysis of the RANS equations, Castillo and George [3] have shown that the proper velocity scale for the outer layer is the outer velocity u_e, rather than the friction velocity. Those authors introduced a modified pressure gradient parameter,

$$\Lambda = \frac{\delta}{\rho_e \, u_e^2 \, \mathrm{d}\delta/\mathrm{d}x} \frac{\mathrm{d}\overline{p}}{\mathrm{d}x}, \tag{3}$$

whose constancy characterizes a different type of boundary layer equilibrium. They showed that most flows are actually in equilibrium (with few exceptions), and surprisingly found that only three values of Λ are possible, namely 0.22, 0 and -1.92, corresponding to adverse-, zero- and favorable-pressure-gradient conditions, respectively. Furthermore,

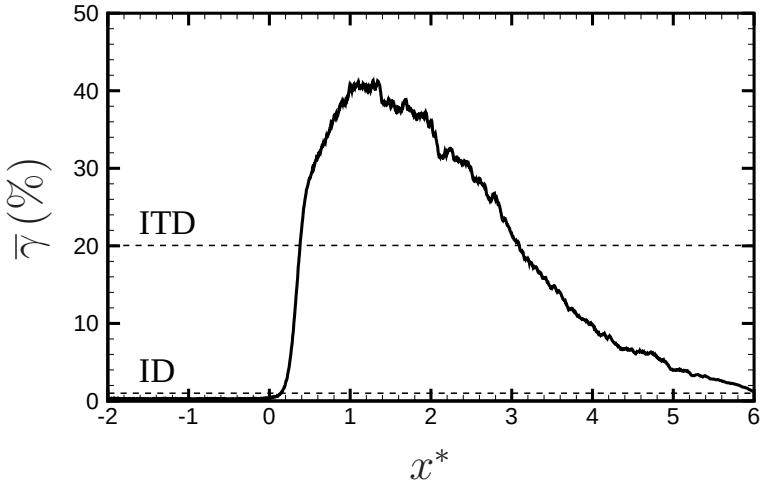

Figure 7: Distribution of the spanwise averaged fraction of time of wall points having $\partial u/\partial y < 0$.

they showed that when the flow is in this equilibrium state, the mean velocity deficit profiles exhibit a collapse when scaled with respect to $u_e\,\delta^*/\delta$, as proposed by Zagarola and Smits [24]. As established by Castillo [2] this scaling effectively removes the effects of both the upstream conditions and finite local Reynolds number on the outer velocity profiles.

If $\Lambda = const$, it is easy to show, upon integration of equation 3 that the boundary layer thickness and the freestream velocity are related through a power-law, i.e.

$$\delta \sim u_e^{-1/\Lambda}. \tag{4}$$

In figure 9 we then report (in logarithmic scale) the freestream velocity u_e normalized by u_∞ as a function of the boundary layer thickness δ normalized by δ_{in}. The figure indeed shows the occurrence of two distinct power-law regions, corresponding, respectively, to the zero-pressure-gradient region upstream of the shock, and the adverse pressure gradient past $x^* \approx 1$, where $\Lambda \approx 0.22$. As shown in figure 10, where the mean van Driest velocity deficit profiles in Zagarola-Smits scaling are reported, the curves collapse quite satisfactorily, except for some deviations observed at $x^* = 1$, where the profile is probably still affected by the flow rearrangement in the interaction zone.

6 CONCLUSIONS

The interaction of a normal shock wave with a turbulent boundary layer under conditions of incipient separation has been analyzed by means of direct numerical simulation of the compressible Navier-Stokes equations. Consistent with experimental observations, the mean flow pattern shows bending of the interacting shock, the formation of an upstream fan of compression waves associated with the thickening of the boundary layer, and the occurrence of a terminating nearly-normal shock, that brings the flow to subsonic conditions. Flow visualizations show that the outer part of the boundary layer is populated by vortical structures, both in the incoming stream and past the interacting shock, where

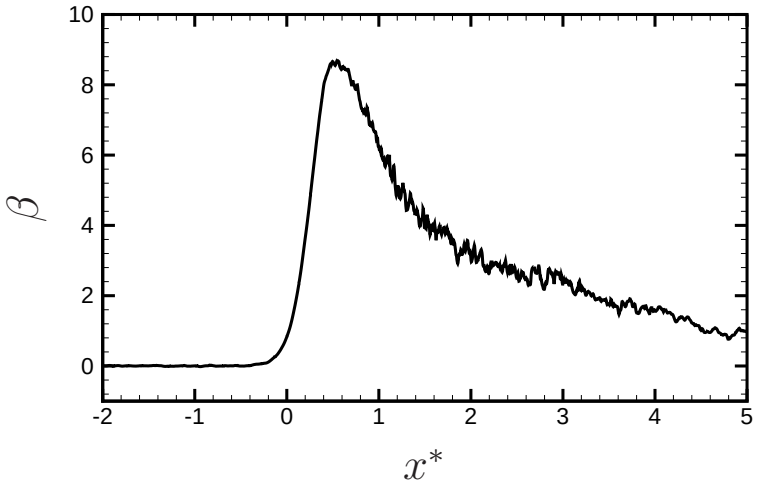

Figure 8: Distribution of Clauser's pressure gradient parameter β as a function of the scaled coordinate x^*.

the mean velocity profile exhibits inflection points, and the flow shows similarities with a turbulent mixing layer. Although at the selected flow conditions no mean separation is observed, the flow is in an 'intermittent transitory detachment' state, exhibiting scattered spots of instantaneous flow reversal throughout the interaction zone. The analysis of the flow recovery past the interacting shock shows that the boundary layer reacts to the adverse pressure gradient by attaining a new equilibrium state over a scale of the order of one interaction length. Such equilibrium state is conveniently described in the framework of the theory of Castillo and George [3]. In particular, in the subsonic adverse-pressure-gradient region, a nearly constant value of the pressure gradient parameter is attained, and the mean velocity defect profiles are very nearly self-similar when reported in the scaling of Zagarola and Smits [24].

References

[1] Bruce, P.J.K.: Transonic shock / boundary layer interactions subject to downstream pressure perturbations. Ph.D. thesis, Magdalene College, Department of Engineering, University of Cambridge (2008)

[2] Castillo, L.: Similarity analysis of turbulent boundary layers. Ph.D. thesis, Ph.D. Dissertation, Dept. of Mechanical and Aerospace Engineering, State Univ. of New York, Buffalo, NY (1997)

[3] Castillo, L., George, W.K.: Similarity analysis for turbulent boundary layer with pressure gradient: Outer flow. AIAA J. **39**, 41–47 (2001)

[4] Clauser, F.H.: Turbulent boundary layers in adverse pressure gradients. J. Aero. Sci. **21**, 91–108 (1954)

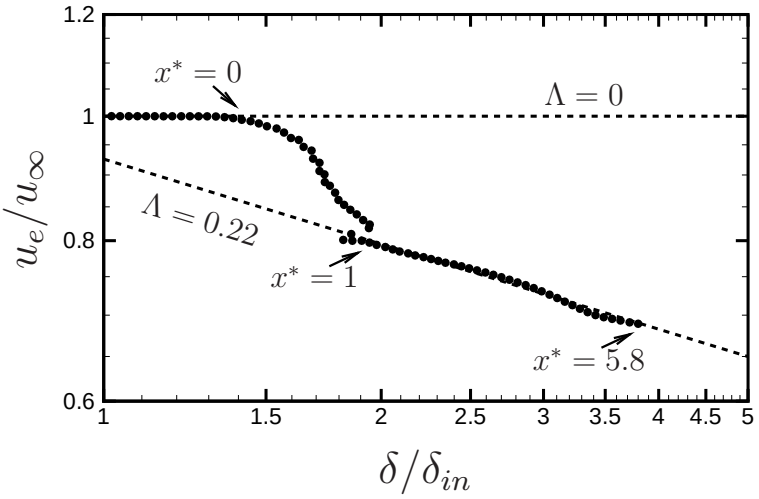

Figure 9: Free-stream velocity u_e/u_∞ as a function of δ/δ_{in}.

[5] Delery, J., Marvin, J.G.: Shock-wave boundary layer interactions. 280, AGARDograph (1986)

[6] Délery, J.M.: Experimental investigation of turbulence properties in transonic shock/boundary layer interactions. AIAA J. **21**, 180–185 (1983)

[7] Dolling, D.S.: Fifty years of shock-wave/boundary layer interaction research: what next? AIAA J **39**, 1517–1531 (2001)

[8] East, L.F.: The application of a laser anemometer to the investigation of shock wave boundary layer interactions. 193, AGARD-CPP (1976)

[9] Green, J.E.: Interactions between shock waves and turbulent boundary layers. Progr. Aerosp. Sci. **11**, 253–340 (1969)

[10] Hopkins, E.J., Inouye, M.: An evaluation of theories for predicting turbulent skin friction and heat transfer on flat plates at supersonic and hypersonic mach numbers. AIAA J. **9**, 993–1003 (1971)

[11] Humble, R.A., Elsinga, G.E., Scarano, F., van Oudheusden, B.W.: Three-dimensional instantaneous structure of a shock/wave turbulent boundary layer interaction. J. Fluid Mech. **622**, 33–62 (2009)

[12] Knight, D., Yana, H., Panaras, A.G., Zheltovodov, A.: Advances in cfd prediction of shock wave turbulent boundary layer interactions. Progr. Aerosp. Sci. **39**, 121–184 (2003)

[13] Na, Y., Moin, P.: Direct numerical simulation of a separated turbulent boundary layer. J. Fluid Mech. **374**, 379–404 (1998)

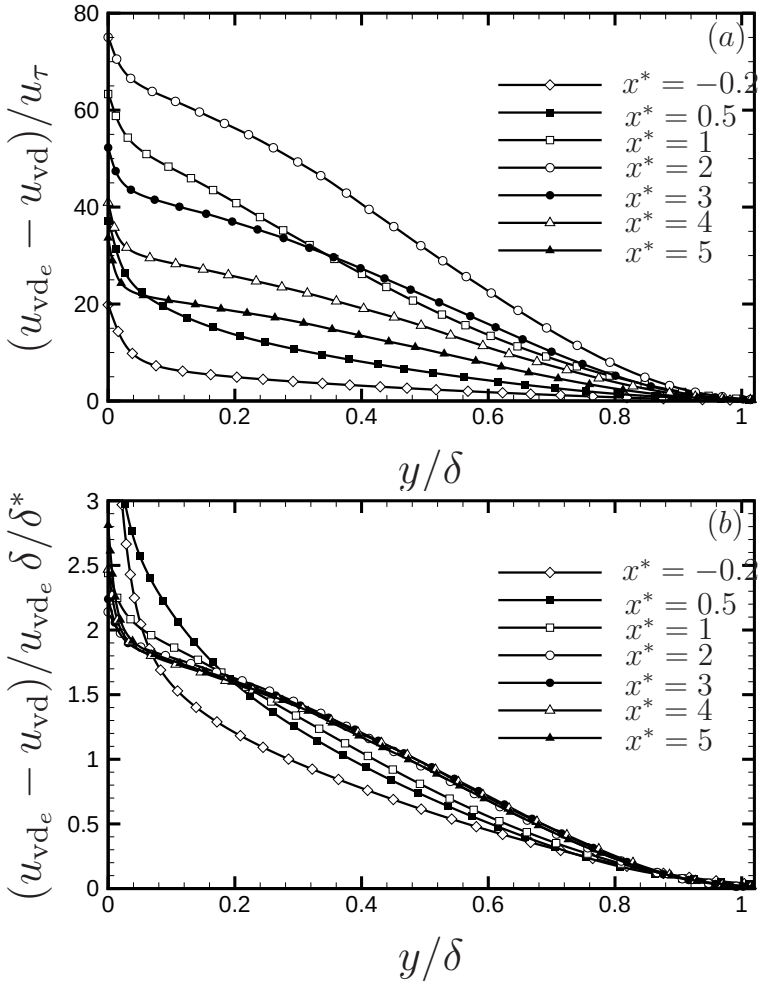

Figure 10: Mean van Driest velocity deficit profiles at several streamwise stations scaled by (a) the friction velocity and (b) in Zagarola-Smits scaling.

[14] Piponniau, S., Dussauge, J.P., Debiéve, J.F., Dupont, P.: A simple model for low-frequency unsteadiness in shock-induced separation. J. Fluid Mech. **629**, 87–108 (2009)

[15] Pirozzoli, S.: Conservative hybrid compact-weno schemes for shock-turbulence interaction. J. Comput. Phys. **178**, 81–117 (2002)

[16] Pirozzoli, S., Bernardini, M., Grasso, F.: Characterization of coherent vortical structures in a supersonic turbulent boundary layer. J. Fluid Mech. **613**, 205–231 (2008)

[17] Pirozzoli, S., Bernardini, M., Grasso, F.: Direct numerical simulation of transonic shock/boundary layer interaction under conditions of incipient separation. J. Fluid Mech. (2010). In press

[18] Pirozzoli, S., Grasso, F.: Direct numerical simulations of isotropic compressible turbulence: Influence of compressibility on dynamics and structures. Phys. Fluids **16**(12), 4386–4407 (2004)

[19] Pirozzoli, S., Grasso, F.: Direct numerical simulation of impinging shock wave turbulent boundary layer interaction at $M = 2.25$. Phys. Fluids **18**, 065,113 (2006)

[20] Sandham, N.D., Yao, Y.F., Lawal, A.A.: Large–eddy simulation of transonic flow over a bump. International Journal of Heat and Fluid Flow **24**, 584–595 (2003)

[21] Simpson, R.L., Chew, Y.T., Shivaprasad, B.G.: The structure of separating turbulent boundary layer. part 1. mean flow and reynolds stresses. J. Fluid Mech. **113**, 23–51 (1981)

[22] Souverein, L., Dupont, P., Debiéve, J., Dussauge, J., van Oudheusden, B., Scarano, F.: Effect of interaction strength on the unsteady behavior of shock wave boundary layer interactions. AIAA Paper 09-3715, AIAA (2009)

[23] Wu, M., Martin, M.: Direct numerical simulation of supersonic turbulent boundary layer over a compression ramp. AIAA J. **45**, 879–889 (2007)

[24] Zagarola, M.V., Smits, A.J.: Mean flow scaling of turbulent pipe flow. J. Fluid Mech. **373**, 33–79 (2000)